CHINESE OPTICS LETTERS

Vol. 21, No. 3 | March 2023

Accurate measurement of aerosol optical properties using the multilongitudinal mode high-spectral-resolution lidar with self-tuning Mach–Zehnder interferometer

Fei Gao (高 飞)[1], Fengjia Gao (高丰佳)[1], Xiao Yang (杨 潇)[1], Gaipan Li (李改盼)[1], Fan Yang (杨 帆)[1], Shichun Li (李仕春)[1], Li Wang (汪 丽)[1], Dengxin Hua (华灯鑫)[1*], and Samo Stanič[2]

[1] School of Mechanical and Precision Instrument Engineering, Xi'an University of Technology, Xi'an 710048, China

[2] Center for Atmospheric Research, University of Nova Gorica, SI-5000 Nova Gorica, Slovenia

*Corresponding author: dengxinhua@xaut.edu.cn

Received September 16, 2022 | Accepted November 7, 2022 | Posted Online January 16, 2023

The multilongitudinal mode (MLM) high-spectral-resolution lidar (HSRL) based on the Mach–Zehnder interferometer (MZI) is constructed in Xi'an for accurate measurements of aerosol optical properties. The critical requirement of the optimal match between the free spectral range of MZI and the longitudinal mode interval of the MLM laser is influenced by the laboratory temperature, pressure, and vibration. To realize the optimal separation of aerosol Mie scattering signals and molecular Rayleigh scattering signals excited by the MLM laser, a self-tuning technique to dynamically adjust the optical path difference (OPD) of the MZI is proposed, which utilizes the maximum ratio between the received power of the Mie channel and Rayleigh channel as the criterion of the OPD displacement. The preliminary experiments show the feasibility of the MLM-HSRL with self-tuning MZI and the stable performance in the separation of aerosol Mie scattering signals and molecular Rayleigh scattering signals.

Keywords: high-spectral-resolution lidar; aerosol optical properties; multilongitudinal mode laser; self-tuning Mach–Zehnder interferometer.

DOI: 10.3788/COL202321.030101

1. Introduction

Aerosol is an important component of air pollutants and one of the most uncertain factors in environmental and climate change, and it is closely related to human activities[1–4]. Accurate measurements of aerosol optical properties can help human understand the dynamic change of atmosphere and provide the theoretical reference for weather forecasting and the analysis of global climate change[5,6].

High-spectral-resolution lidar (HSRL) has proven to be a powerful tool for the measurement of aerosol optical properties[7,8], which uses the seeded high-power pulsed laser as the excitation light source, and chooses the narrowband filters (atomic/molecular absorption filter or interferometer optical filter) as the spectral discriminator to separate aerosol Mie scattering signals and molecular Rayleigh scattering signals excited by single-frequency laser pulses[9,10]. The concept of the multilongitudinal mode (MLM) HSRL has been proposed recently[11–14], which abandons the employment of the complex seeded laser techniques, and directly utilizes the high-power pulsed laser with the MLM laser as the excitation light source. Different from the single-frequency HSRL, the MLM-HSRL can only use the optical interferometer with the periodic transmittance function as the spectral discriminator to separate aerosol Mie scattering signals and molecular Rayleigh scattering signals excited by the MLM laser pulses.

Xi'an University of Technology has been developing an MLM-HSRL for aerosol measurements that uses a tunable Mach–Zehnder interferometer (MZI) with a large optical path difference (OPD) as the spectral discriminator[15]. However, the optical match between the free spectral range (FSR) of MZI and the longitudinal mode interval of the MLM laser is frequently influenced by external environmental factors such as laboratory temperature, pressure, and vibration, which leads to a worse discrimination effect of aerosol Mie scattering signals and molecular Rayleigh scattering signals. In order to enhance the discrimination capability of the MZI with large OPD in the MLM-HSRL system, we develop an MZI with self-tuning functionality of the OPD that achieves the dynamic match in nanometer magnitude between the FSR of MZI and the longitudinal mode interval of the MLM lasers by using the piezoelectric ceramic nanodisplacement platform. In this paper, we present

the techniques of the MLM-HSRL with self-tuning MZI and its preliminary measurements of aerosol optical properties.

2. Setup of the MLM-HSRL and Data Retrieval

The MLM-HSRL system based on the self-tuning MZI is shown in Fig. 1. The Nd:YAG high-power pulsed laser with a wavelength of 532 nm and a pulse energy of 150 mJ at the repetition rate of 10 Hz is used as the transmitter. The number of longitudinal modes is 101, the mode interval is 300 MHz at the radiation linewidth of 30 GHz, and the length of the laser resonator is 500 mm. A Cassegrain telescope is employed to receive the lidar echo signals excited by the MLM laser pulses, which has a receiving aperture of 203 mm and a focal length of 2000 mm. A self-tuning MZI with the OPD of 1000 mm is designed as the spectral discriminator to separate aerosol Mie scattering signals and molecular Rayleigh scattering signals. A Tektronix oscilloscope is chosen for data acquisition with analog detection mode of the real-time sampling rate of 125 MS/s, resulting in the range resolution of 1.5 m in the raw data profile.

The tunable MZI is the key component in the design of the MLM-HSRL, which is composed of lenses, beam splitters (BSs), Dove prisms, a displacement system, field compensation glasses (FCGs), and photomultiplier tubes (PMTs). Lens1 collimates the MLM echo signals from the multimode fiber with a diameter of 0.8 mm, which is utilized to transfer the received backscattered light from telescope to the spectral discriminator MZI. The beam splitter BS1 divides the MLM echo signals into two parts. The reflected signals of BS1 are reflected 3 times by the Dove prisms (Prism3, Prism4, Prism5) and then reach the beam splitter BS2, which constructs the long optical path of the MZI. Field compensation glasses (FCG1, FCG2, FCG3, and FCG4) with a total length of 1165.767 mm are added to the long optical path to expand the receiving field of view of the MZI up to 5 mrad. The transmitted signals of BS1 are reflected twice by the Dove prisms (Prism1 and Prism2) and then reach the beam splitter BS2, which constructs the short optical path of the MZI. The Prism1 of the short optical path is mounted on the displacement system, which changes the short optical path of the MZI by moving the Prism1 forward and backward. The OPD of MZI can be changed with the movement precision of centimeter, millimeter, and nanometer by different displacement platforms, respectively.

The MZI has two channels with the complementary output signals; one channel transmits aerosol Mie scattering signals and is called the Mie channel; the other channel suppresses aerosol Mie scattering signals and is called the Rayleigh channel. The spectra of the MLM laser, lidar echo signal, and the outputs of the Mie channel and Rayleigh channel are plotted in Fig. 1 as well, to show the working principle of the MLM-HSRL. The lidar equations for both the Mie channel and the Rayleigh channel of the MLM-HSRL can be expressed as

$$\begin{cases} P_{\mathrm{a}}(r) = CP_0 r^{-2}[T_{\mathrm{aa}}\beta_{\mathrm{a}}(r) + T_{\mathrm{am}}\beta_{\mathrm{m}}(r)]\exp\left\{-2\int_0^r[\alpha_{\mathrm{a}}(r') + \alpha_{\mathrm{m}}(r')]\mathrm{d}r'\right\} \\ P_{\mathrm{m}}(r) = CP_0 r^{-2}[T_{\mathrm{ma}}\beta_{\mathrm{a}}(r) + T_{\mathrm{mm}}\beta_{\mathrm{m}}(r)]\exp\left\{-2\int_0^r[\alpha_{\mathrm{a}}(r') + \alpha_{\mathrm{m}}(r')]\mathrm{d}r'\right\} \end{cases}, \tag{1}$$

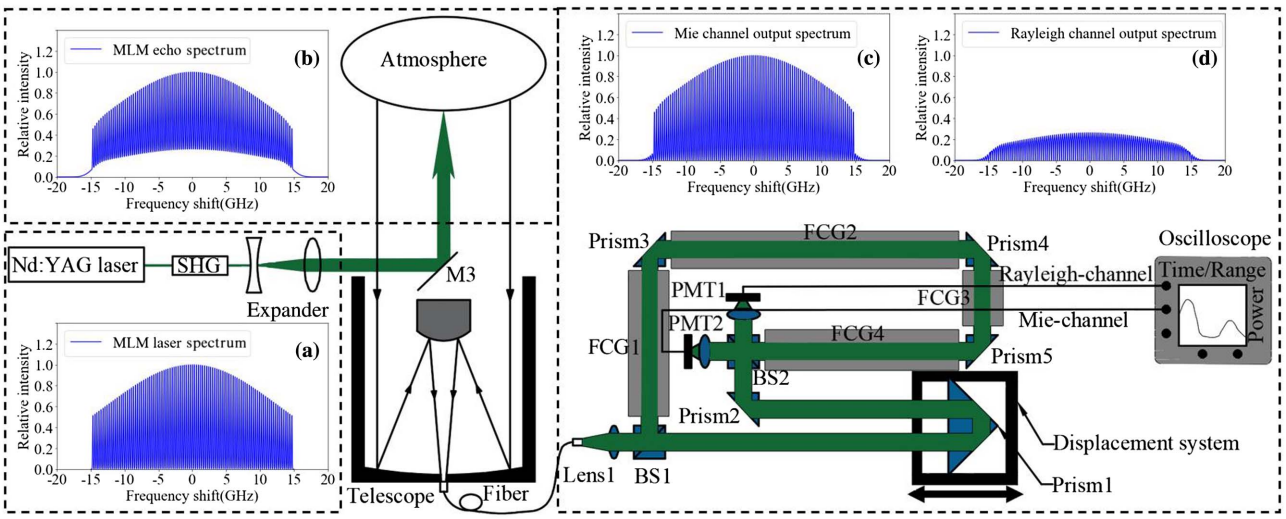

Fig. 1. Schematic diagram of the multilongitudinal mode HSRL system: (a) spectrum of the MLM laser; (b) spectrum of the MLM echo signal; (c) output spectrum of the Mie channel of the MZI; (d) output spectrum of the Rayleigh channel of the MZI.

where $P_a(r)$ and $P_m(r)$ represent the instantaneous received power of the Mie channel and the Rayleigh channel, and their summation presents the total lidar return signals $P(r)$. r is the distance from the laser echo signals to the telescope. C is the lidar system constant. P_0 is the transmitted laser power. T_{ax} and T_{mx} are the effective transmittance of the Mie channel and the Rayleigh channel for aerosol Mie scattering signals ($x = a$) or molecular Rayleigh scattering signals ($x = m$), respectively. $\beta_a(r)$ and $\beta_m(r)$ are the volume aerosol backscattering coefficient and molecular backscattering coefficient. $\alpha_a(r)$ and $\alpha_m(r)$ are the volume aerosol extinction coefficient and molecular extinction coefficient. The aerosol optical properties of $\beta_a(r)$ and $\alpha_a(r)$ using the MLM-HSRL can be retrieved as

$$\beta_a(r) = \frac{T_{mm}P_a(r) - T_{am}P_m(r)}{T_{aa}P_m(r) - T_{ma}P_a(r)}\beta_m(r), \tag{2}$$

$$\alpha_a(r) = -\frac{1}{2}\frac{d}{dr}\left\{\ln\frac{r^2[P_a(r) + P_m(r)]}{CP_0[\beta_a(r) + \beta_m(r)]}\right\} - \alpha_m(r), \tag{3}$$

where $\beta_m(r)$ and $\alpha_m(r)$ can be obtained through the standard atmospheric model.

Based on the retrieval algorithm of aerosol optical properties using the MLM-HSRL, the retrieval accuracy is highly related to the effective transmittance (T_{aa} and T_{ma}) of the MZI, which is the function of the complex degree of coherence[16]. In order to obtain the reliable retrieval results with relative error within 20%, the relative error of T_{aa} needs be controlled within 10%. The effective transmittance of the MZI is mostly affected by the OPD of the MZI when considering that the longitudinal mode interval is kept constant. The optimal setting of the OPD of MZI must meet two conditions:

$$\begin{cases} \text{OPD} = 2L \\ \text{OPD} = k\lambda, k \in \mathbb{N}^* \end{cases}, \tag{4}$$

where OPD is the optical path difference of the MZI, L is the laser optical cavity length, λ is the laser wavelength, and $\mathbb{N}^*$ is the set of positive integers ($k = 1, 2, 3 \ldots$). When the laser optical cavity length is 500 mm, the optimal setting of the OPD should be 1000 mm to satisfy the first condition.

Theoretical analysis shows that the maximum value of T_{aa} is 0.837 at the MZI OPD of 1000 mm, and the values of T_{aa} are greater than 0.800 (the relative error of T_{aa} is smaller than 10%) when the OPD of MZI is between 999 and 1001 mm, which shows that the accuracy of the OPD of the MZI should be controlled within ±1 mm to satisfy the first condition [Fig. 2(a)]. Moreover, in the second condition with the periodic cosine variation of T_{aa} with the period of laser wavelength of 532 nm, theoretical analysis shows that the values of T_{aa} are greater than 0.800 when the OPD of the MZI is between 999.99983 and 999.99991 mm, which shows that the accuracy of the OPD of the MZI should be controlled within ±40 nm to satisfy the second condition [Fig. 2(b)].

Theoretical calculation shows that the temperature accuracy and pressure accuracy of the MZI and laser cavity should be

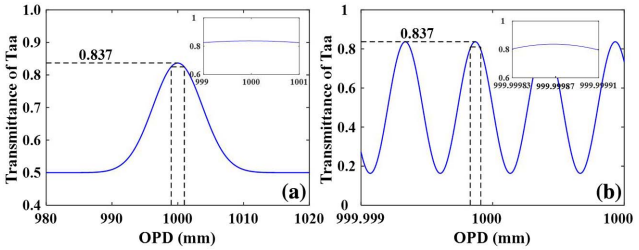

Fig. 2. Relationship between the effective transmittance of the Mie channel for Mie scattering signals and the OPD of the MZI. (a) For the first condition of the matching degree between the MZI OPD and the laser optical cavity length; (b) for the second condition of the matching degree between the MZI OPD and laser wavelength.

controlled within ±0.003°C and ±0.0002 atm. However, it is difficult to realize the temperature and pressure control, considering both the MZI and the laser cavity have a big volume, especially in the open atmosphere during the experiments using the MLM-HSRL. For such a consideration, a self-tuning MZI system with the OPD variation accuracy of nanometer magnitude is designed in the MLM-HSRL, aiming to optimize the matching degree between the FSR of MZI and the longitudinal mode interval of the laser and to obtain the optimal separation of aerosol Mie scattering signals and molecular Rayleigh scattering signals.

The functional diagram and the flow chart of the MLM-HSRL with a self-tuning MZI are shown in Fig. 3. The data acquisition and processing system is used not only to record the complementary outputs of the Mie channel and the Rayleigh channel, but also to connect with the proportional integral (PI) controller for the nanodisplacement platform, which can adjust the OPD of the MZI in nanometer magnitude. Theoretical simulations show that the ratio (P_Δ) between the outputs of the Mie channel (P_a) and Rayleigh channel (P_m) has a maximum value when there is an optimal match between the FSR of the MZI and the longitudinal mode interval of the laser; therefore, the criterion of the displacement correction of the OPD of the MZI is set as

$$\max = \sum_h \left[\frac{P_a(r)}{P_m(r)}\right] = \sum_h (P_\Delta). \tag{5}$$

Considering that the data are collected by means of analog detection mode, and the recorded data of both the Mie channel and the Rayleigh channel are the profiles related to the atmospheric information, the probing data within the detection range h (SNR ≥ 10) are used to calculate P_Δ for comparison. The forward or backward movement of the nanodisplacement platform is judged by the previous $P_{\Delta 1}$ [defined as "a" in Fig. 3(b)] and the measured $P_{\Delta 2}$ [defined as "b" in Fig. 3(b)], which should be assigned as "a" if the value of $P_{\Delta 2}$ is greater than the value of $P_{\Delta 1}$. During the whole measurement, the nanodisplacement platform is dynamically moved forward and backward to search for the optimal position of the OPD of the MZI, for realizing the

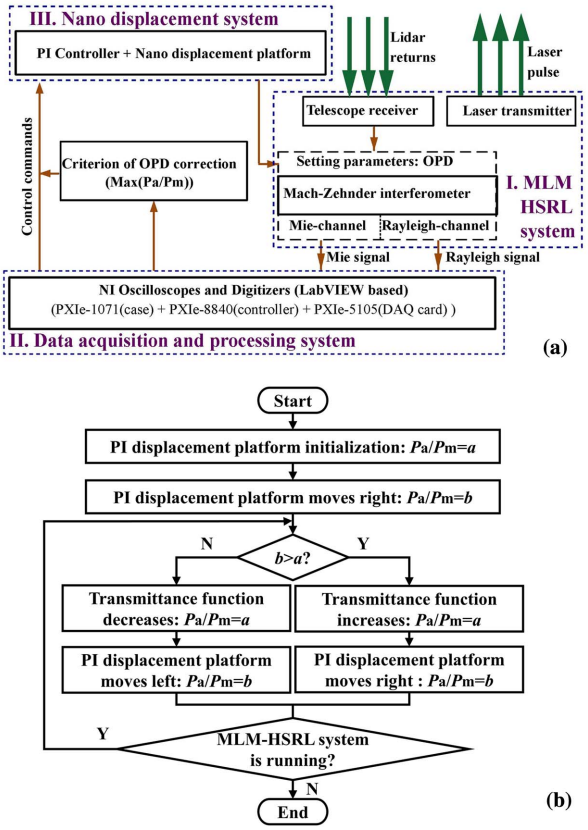

Fig. 3. (a) Functional diagram and (b) flow chart of the MLM-HSRL with a self-tuning MZI.

optimal spectral discrimination between aerosol Mie scattering signals and molecular Rayleigh scattering signals.

3. Preliminary Experiments

After the construction of the MLM-HSRL with the self-tuning MZI, the preliminary experiments are performed in Xi'an to verify the feasibility of the MLM-HSRL and the performance of the self-tuning MZI. For quick self-tuning functionality applied in the MZI and maximum detection range of the MLM-HSRL, each profile is a summation result of 30 s (300 laser shots). Figure 4 shows the P_Δ distribution measured by the MLM-HSRL with the fixed-OPD MZI from 19:30 CST to 21:05 CST on March 9, 2022. From the time height indicator (THI) contour diagram of P_Δ distribution [Fig. 4(a)], it can be seen that the value of P_Δ is changed not only with the time, but also with the height. The variation of P_Δ with time could be explained by the mismatch between the FSR of the MZI and the longitudinal mode interval of the laser during the measurement period, while the variation of P_Δ with height could be due to the decrement of T_{aa} and increment of T_{ma}, especially for the aerosol layer at the heights of 300–900 m and the cloud layer at the heights of 3000–4000 m. The statistics of P_Δ in Fig. 4(b) shows the P_Δ is distributed with the bimodal distribution and mostly distributed in the interval of 2.0–2.5.

Figure 5 shows the P_Δ distribution measured by the MLM-HSRL with the dynamic OPD MZI from 21:30 CST to 22:55 CST on March 9, 2022, which means that the self-tuning functionality is applied during the measurements. From both the THI contour diagram of P_Δ in Fig. 5(a) and the statistics

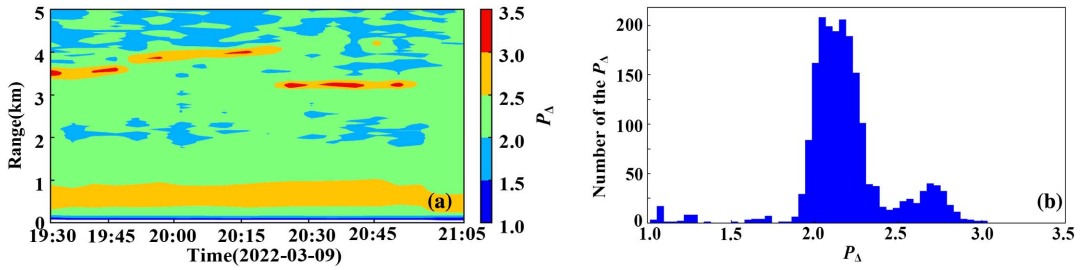

Fig. 4. P_Δ distribution from the preliminary experiments by the MLM-HSRL with the fixed OPD MZI performed from 19:30 CST to 21:05 CST on March 9, 2022. (a) THI contour diagram of P_Δ; (b) statistics diagram of P_Δ.

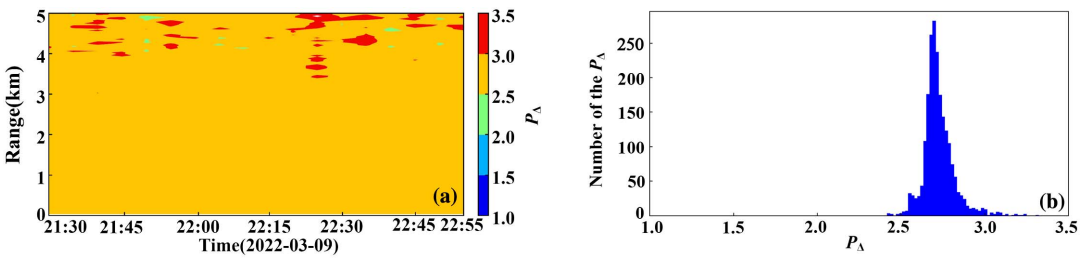

Fig. 5. P_Δ distribution from the preliminary experiments by the MLM-HSRL with the dynamic OPD MZI performed from 21:30 CST to 22:55 CST on March 9, 2022. (a) THI contour diagram of P_Δ; (b) statistics diagram of P_Δ.

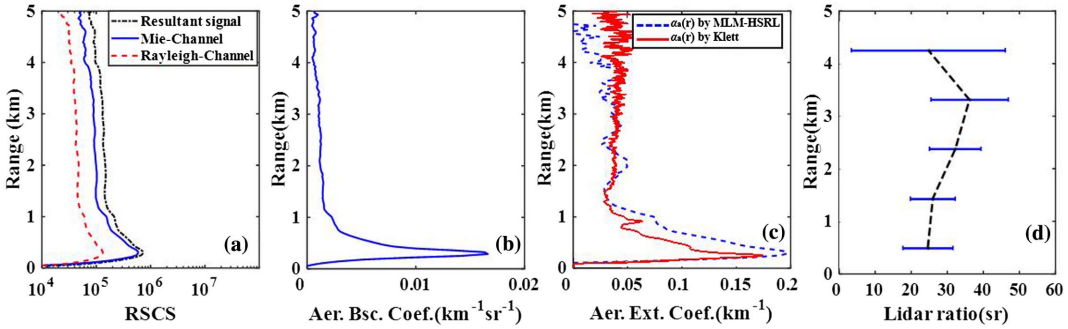

Fig. 6. Example of the preliminary experimental data using the MLM-HSRL and the retrieval results of aerosol optical properties during a clear weather condition performed at 21:50 CST on March 12, 2022. (a) Profile of RSCS data; (b) profile of $\beta_a(r)$; (c) profile of $\alpha_a(r)$; (d) profile of lidar ratio.

diagram of P_Δ in Fig. 5(b), it can be seen that most values of P_Δ are distributed within the interval of 2.5–3.0. Compared with the distribution of P_Δ in the fixed OPD system, the distribution of P_Δ in the dynamic OPD system is relatively more concentrated, and the values of P_Δ are also larger than in the fixed-OPD system, meaning that the transmittance of the MZI is almost kept constant to separate aerosol Mie scattering signals and molecular Rayleigh scattering signals after self-tuning. The phenomenon that some values are larger than 3.0 above the height of 4000 m could be due to the low signal-to-noise ratio.

The examples of the preliminary experimental profiles and the corresponding retrieval results of aerosol optical properties from the self-tuning MLM-HSRL system are shown in Figs. 6 and 7, which were taken at a clear weather condition at 21:50 CST on March 12, 2022 (Fig. 6) and at a cloudy weather condition at 21:20 CST on April 13, 2022 (Fig. 7), respectively. In both weather conditions, the range-square-corrected signal (RSCS) data from the Rayleigh channel is smaller than the RSCS data from the Mie channel by one order of magnitude, which is due to the suppression of Mie scattering signals in the Rayleigh channel and can be explained by the values of T_{aa} and T_{ma}. However, the Rayleigh channel cannot suppress aerosol Mie scattering signals totally, which can be seen from the cloud layer (the bulge in the profile of the RSCS above the atmospheric boundary layer is taken as the cloud layer) at the height of 3 km during the cloudy weather condition [Fig. 7(a)]. Aerosol optical properties, including the $\beta_a(r)$, $\alpha_a(r)$, and lidar ratio, can be retrieved from the RSCS data in both weather conditions. In the clear weather condition (Fig. 6), there is an aerosol layer within 1 km, which can be seen from all the profiles of RSCS, $\beta_a(r)$, and $\alpha_a(r)$. More fluctuations appear in the profile of $\alpha_a(r)$ with the maximum value of 0.20 km^{-1} than in the profile of $\beta_a(r)$ with the maximum value of 0.016 km^{-1} sr^{-1} within 1 km, which could be due to the differential algorithm in the retrieval of $\alpha_a(r)$ and aerosol characteristics (aerosol layer at 1.0 and 2.0 km). In the cloudy weather condition (Fig. 7), there is an aerosol layer with wide distribution within 1.5 km and a thick cloud layer at the height of 3 km. The retrieval results of $\beta_a(r)$ at the cloud layer with a maximum value of 0.005 km^{-1} sr^{-1} are slightly larger than that at the aerosol layer with a maximum value of 0.004 km^{-1} sr^{-1}, indicating that the density of the cloud layer is relatively high. The retrieval results of the lidar ratio, which fluctuate between 20 and 40 sr in the clear weather [Fig. 6(d)] and between 10 and 20 sr in the cloudy weather, are mostly due to the different aerosol types. The self-tuning technique on the OPD of the MZI can keep the relative error of T_{aa} smaller than 10%, so the retrieval results are reliable. Meanwhile, $\alpha_a(r)$ retrieved by the Klett method using the resultant signals $P(r)[=P_a(r) + P_m(r)]$ is plotted in Figs. 6(c) and 7(c) as well, which has a good agreement with the retrieval results by the MLM-HSRL.

The THI diagrams of the retrieved $\beta_a(r)$ and $\alpha_a(r)$ from the performed experiments at the time interval of 21:30 CST to 22:55 CST on March 9, 2022 are shown in Fig. 8. The contour

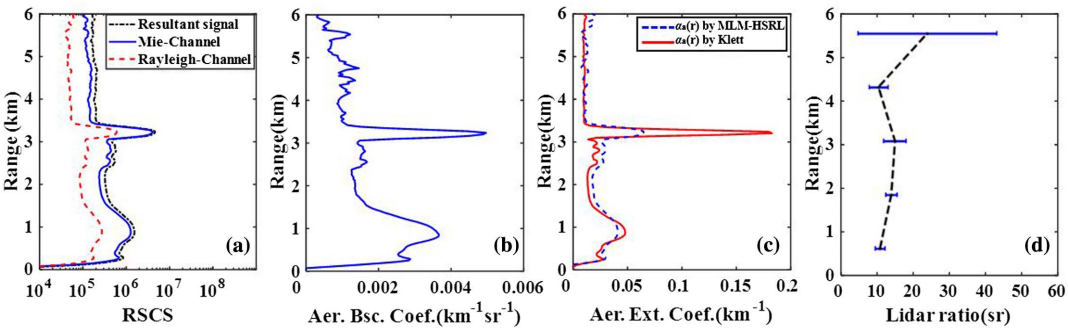

Fig. 7. Example of the preliminary experimental data using the MLM-HSRL and the retrieved results of aerosol optical properties during a cloudy weather condition performed at 21:20 CST on April 13, 2022. (a) Profile of RSCS data; (b) profile of $\beta_a(r)$; (c) profile of $\alpha_a(r)$; (d) profile of lidar ratio.

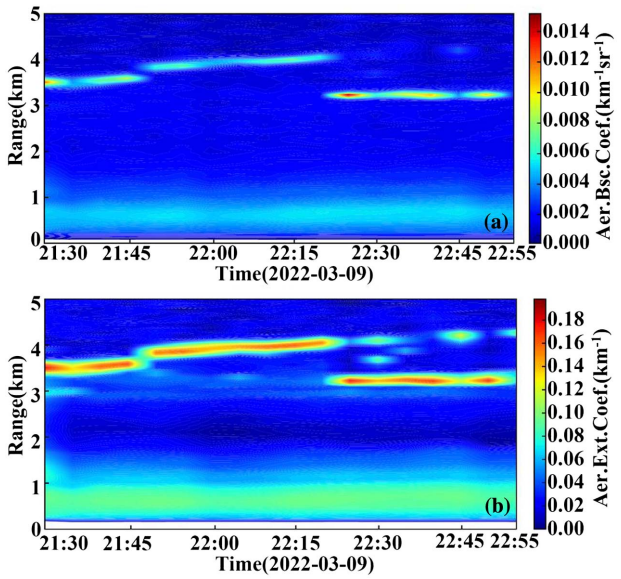

Fig. 8. THI diagram of the retrieval results of aerosol optical properties from 21:30 CST to 22:55 CST on March 9, 2022. (a) $\beta_a(r)$; (b) $\alpha_a(r)$.

of aerosol layer at the height of 0–1 km and cloud layer at the height of 3–4 km shows the variation trend of aerosol and cloud optical characteristics with time. The contour diagram of P_Δ and the statistical diagram of P_Δ are checked as well for the continuous measurements, which show the values of P_Δ distributed within the interval of 2.5–3.0 as well (similar to Fig. 5). The preliminary experiments using the MLM-HSRL system show that the designed MLM-HSRL with the self-tuning MZI has relatively stable detection performance.

4. Conclusions

The MLM-HSRL with the self-tuning MZI was constructed at the Xi'an University of Technology for aerosol measurements. Compared with the single-frequency HSRL, the MLM-HSRL technique abandons the complex techniques of laser seeding and frequency stabilization, although the MLM-HSRL technique can provide a relatively lower spectral discrimination ratio (T_m/T_a), which is deduced from the value of T_{aa} and the experimental data from both the aerosol layer and the cloud layer. To realize the critical requirement of the stable match between the FSR of the MZI and the longitudinal mode interval of the MLM laser, a self-tuning technique is applied to dynamically adjust the OPD of the MZI, which uses the maximum ratio of the received power of the Mie channel and the Rayleigh channel as the criterion of the OPD displacement correction. The PI controller controls the nanodisplacement platform, moving with 20 nm step precision within a wavelength range of 532 nm to realize the self-tuning of the MZI OPD, which takes about 15 min in real measurements to find the optimal OPD. Theoretical calculation shows that the optimal value of P_Δ is 2.94 (the ratio of T_{aa} and T_{ma}) when the FSR of the MZI is 300 MHz. The values of P_Δ in the preliminary experiment results using the MLM-HSRL are mainly distributed between 2.5 and 3.0 after the self-tuning application, which is slightly smaller than the value by theoretical calculation and can be explained by the decreased suppression rate of the Rayleigh channel for aerosol Mie scattering signals. In addition, preliminary experimental observations based on the self-tuning MLM-HSRL system show that the constructed system can perform accurate measurements of aerosol optical properties within 5 km in both clear and cloudy weather conditions. To conclude, the MLM-HSRL system with a self-tuning MZI is a novel and reliable remote-sensing technique in accurate measurements of aerosol optical properties.

Acknowledgement

This work was supported by the National Natural Science Foundation of China (Nos. 42175149 and 41775035), the China-CEEC Joint Higher Education Project (No. 202017), and the Natural Science Foundation of Shaanxi Province, China (No. 2020JM-445).

References

1. M. Casazza, M. Lega, G. Liu, S. Ulgiati, and T. A. Endreny, "Aerosol pollution, including eroded soils, intensifies cloud growth, precipitation, and soil erosion: a review," J. Cleaner Prod. **189**, 135 (2018).
2. L. Simone, M. Fabio, R. Marco, C. R. James, and W. J. Ellsworth, "Impact of varying lidar measurement and data processing techniques in evaluating cirrus cloud and aerosol direct radiative effects," Atmos. Meas. Tech. **11**, 1639 (2018).
3. Q. Liu, X. C. Jia, J. N. Quan, J. Y. Li, X. Li, Y. X. Wu, D. Chen, Z. F. Wang, and Y. G. Liu, "New positive feedback mechanism between boundary layer meteorology and secondary aerosol formation during severe haze events," Sci. Rep. **8**, 6095 (2018).
4. Y. Zhang, J. Tao, N. Ma, Y. Kuang, and H. Su, "Predicting cloud condensation nuclei number concentration based on conventional measurements of aerosol properties in the North China Plain," Sci. Total Environ. **719**, 137473 (2020).
5. X. Yu, B. Zhu, and M. Zhang, "Seasonal variability of aerosol optical properties over Beijing," Atmos. Environ. **43**, 4095 (2009).
6. V. A. Kovalev and W. E. Eichinger, *Elastic Lidar* (John Wiley & Sons, 2004).
7. S. Lolli, E. J. Welton, J. R. Campbell, E. Eloranta, and S. V. Salinas, "High spectral resolution lidar and MPLNET micro pulse lidar aerosol optical property retrieval intercomparison during the 2012 7-SEAS field campaign at Singapore," Proc. SPIE **9246**, 92460C (2014).
8. J. Ren, W. Tan, X. Tian, Z. Wu, and T. Zhu, "Retrieval of aerosol liquid water content from high spectral resolution lidar," Sci. Total Environ. **799**, 149423 (2021).
9. X. Shen, N. Wang, I. Veselovskii, D. Xiao, and D. Liu, "Development of ZJU high-spectral-resolution lidar for aerosol and cloud: calibration of overlap function," J. Quant. Spectrosc. Radiat. Transfer **257**, 107338 (2020).
10. S. Li, H. Di, Q. Wang, G. Han, and Y. Li, "Retrieval of the aerosol extinction coefficient of 1064 nm based on high-spectral-resolution lidar," J. Quant. Spectrosc. Radiat. Transfer **256**, 107298 (2020).
11. Y. Jin, N. Sugimoto, T. Nishizawa, P. Ristori, and L. Otero, "A concept of multi-mode high spectral resolution lidar using Mach Zehnder interferometer," EPJ Web Conf. **119**, 02006 (2016).
12. P. Ristori, L. Otero, Y. Jin, N. Sugimoto, T. Nishizawa, and E. Quel, "Development of a high spectral resolution lidar using a multi-mode laser and a tunable interferometer," EPJ Web Conf. **119**, 06005 (2016).

13. Y. Jin, N. Sugimoto, P. Ristori, T. Nishizawa, and E. Quel, "Measurement method of high spectral resolution lidar with a multimode laser and a scanning Mach Zehnder interferometer," Appl. Opt. **56**, 5990 (2017).
14. Z. Cheng, D. Liu, Y. Zhang, C. Liu, and L. Yang, "Generalized high spectral resolution lidar technique with a multimode laser for aerosol remote sensing," Opt. Express **25**, 979 (2017).
15. F. Gao, H. Nan, R. Zhang, Q. Zhu, and S. Stanič, "Quasi-monochromatic of laser echo signals on transmittance of Mach–Zehnder interferometer for UV multi-longitudinal-mode high-spectral-resolution lidar," J. Quant. Spectrosc. Radiat. Transf. **234**, 10 (2019).
16. F. Gao, T. Chen, K. J. Chen, R. Zhang, L. Wang, J. J. Liu, D. X. Hua, and S. Stanič, "A novel retrieval algorithm of multi-longitudinal-mode high-spectral-resolution lidar based on complex degree of coherence and the analyses of absolute errors," J. Quant. Spectrosc. Radiat. Transfer **272**, 107829 (2021).